AGU PUBLICATIONS

Global Biogeochemical Cycles

RESEARCH ARTICLE
10.1002/2013GB004568

Key Points:
- Desert bedrock fractures contain substantial amounts of carbonate
- The upper 2 m of analyzed exposures host about 0.079 mTC per square meter
- Pilot data suggest an asymmetric rhythm of storage and release of this carbon

Correspondence to:
E. J. Harrison,
emma.harrison@asu.edu

Citation:
Harrison, E. J., and R. I. Dorn (2014), Introducing a terrestrial carbon pool in warm desert bedrock mountains, southwestern USA, *Global Biogeochem. Cycles*, *28*, 253–268, doi:10.1002/2013GB004568.

Received 11 JAN 2013
Accepted 30 JAN 2014
Accepted article online 6 FEB 2014
Published online 17 MAR 2014

Introducing a terrestrial carbon pool in warm desert bedrock mountains, southwestern USA

Emma J. Harrison[1] and Ronald I. Dorn[1]

[1]School of Geographical Sciences and Urban Planning, Arizona State University, Tempe, Arizona, USA

Abstract Growth of the Phoenix metropolitan area led to road cut or house platform exposures of the internal bedrock material of surrounding semiarid mountain ranges. Similar exposures in the surrounding Sonoran and Mojave Deserts reveal the presence of sedimentary calcium carbonate infilling the preexisting fracture matrix of the bedrock. Field surveys at 31 sites with bedrock fractures filled with carbonate, referred to as BFFC in the following text, reveal an average of 0.079 ± 0.036 mTC/m^2 stored in the upper 2 m of analyzed bedrock exposures. Backscattered electron microscopy images indicate the presence of carbonate at the micron scale, not included in this estimate of carbon storage. Pilot radiocarbon and Sr isotope analyses suggest that one of the surveyed BFFC veins was flushed into the bedrock from a nonbedrock source during the wetter last glacial period in the late Pleistocene.

1. Introduction

Paleoclimatic proxy records reveal that atmospheric CO_2 concentrations fluctuated between 200 and 280 ppm over the past 40,000 years, while current atmospheric CO_2 levels have reached >100 ppm above this natural variability [*Falkowski et al.*, 2007]. The historic flux of CO_2 into the atmosphere derives from short-term sources, such as fossil fuel combustion and changes in land cover biomass [*Liu et al.*, 2003]. Earth, thus, faces a pressing crisis related to atmospheric carbon dioxide management [*Sundquist et al.*, 2008, 2009].

Over geological timescales ocean-lithosphere-atmosphere carbon exchanges tended to be balanced by rates of weathering and geologic CO_2 emissions [*Sundquist*, 1993]. Decay of calcium-bearing silicates led to geological storage of carbonates via the *Urey* [1952] reaction. This process is considered to be one of the most important for reducing atmospheric CO_2 over geologic timescales of millions of years [*Schwartzman*, 1999]. However, the rate of carbon dioxide drawdown by this process has been considered too slow to cope with the rapid modern increases in CO_2 [*McPherson and Sundquist*, 2009; *Suchet et al.*, 2003]. This assumption is being challenged by recent research suggesting that CO_2 consumption from dissolution of pedogenic/secondary carbonate minerals has been greatly underestimated and could be a key driver of annual to decadal changes in climate [*Jacobson et al.*, 2002b; *Lerman and MacKenzie*, 2005; *Liu et al.*, 2010, 2011]. In addition, understanding exchanges between CO_2 stored in carbonates and the atmosphere is an issue of consequence to the critical zone, the active interface between the lithosphere, atmosphere, and biota [*Amundson et al.*, 2007; *Brantley et al.*, 2007; *Derry and Chadwick*, 2007] that stores about ~1600 Gt of organic carbon and ~900 Gt of carbon as carbonate [*Eswaran et al.*, 1993, 1999; *Falkowski et al.*, 2007; *Lal*, 2004, 2008; *Schlesinger*, 1982; *Sundquist*, 1993].

While pedogenic and regolith carbonate in the upper few meters of the lithosphere is a relatively small piece in the global carbon cycle, these deposits are both widespread and abundant, especially in what are now hyperarid, arid, and semiarid settings. These carbonate deposits exist as pedogenic calcrete [*Schlesinger*, 1982, 1985; *Sombroek et al.*, 1993] and regolith carbonates [*Dart et al.*, 2007; *Hill et al.*, 1998; *McQueen et al.*, 1999] that include a wide range of deposits that can form through processes other than pedogenesis.

Calcium carbonate deposits seen as infilled bedrock fractures, which will be referred to in this text as "bedrock fractures filled with carbonate" (BFFC) occur in a variety of global settings (Figure 1). The explosive population growth in the southwestern USA, combined with the mindset of urban sprawl, has led to a great many exposures of bedrock cut through mountains and also bedrock pediments (Figure 2), or low-relief erosion surfaces fronting ranges [*Dohrenwend and Parsons*, 2009]. Both landforms—mountain ranges and pediments—represent the same sort of carbon pool where carbonates infuse into fractures in bedrock. The focus of this paper rests in assessing the potential magnitude of carbon in the BFFC pool. We hypothesize

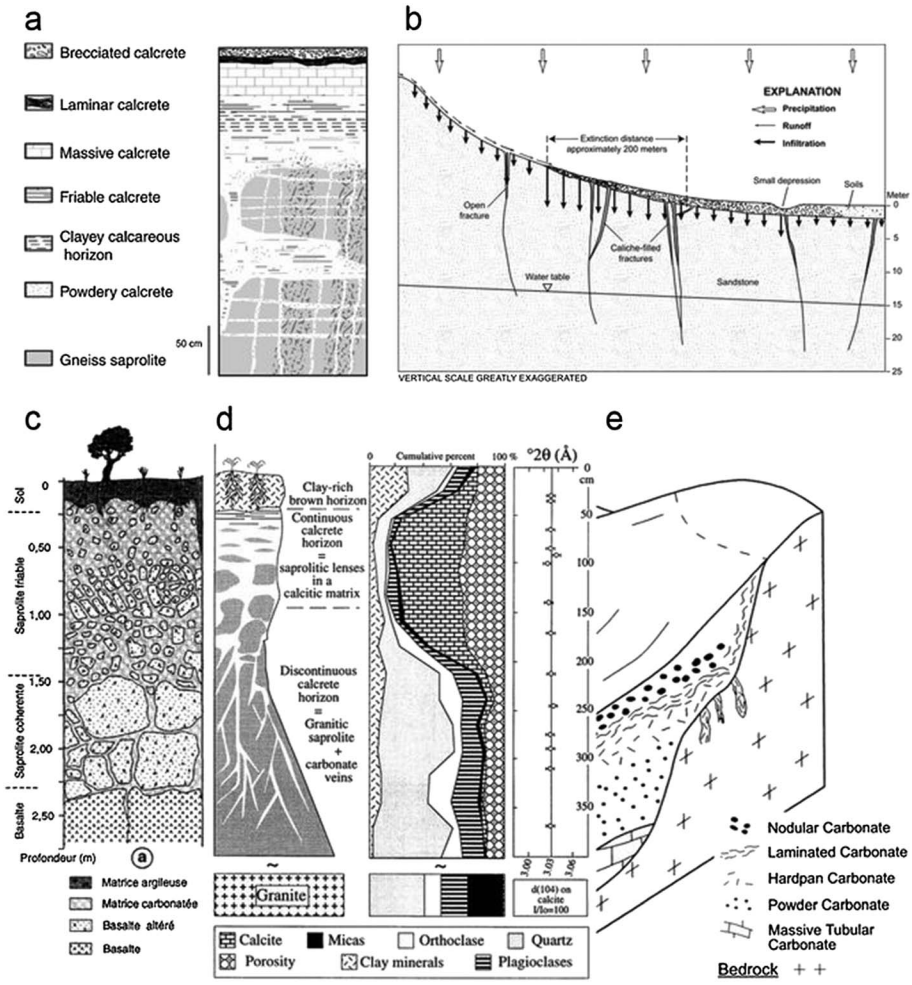

Figure 1. Diagrams showing veins of carbonate penetrating into bedrock (a) gneiss in south India [*Durand et al.*, 2006], (b) sandstone in Utah, USA [*Heilweil et al.*, 2007], (c) basalt in the Middle Atlas of Morocco [*Hamidi et al.*, 1999], (d) granite in central Spain [*Chiquet et al.*, 1999], and (e) varied lithologies in southeastern Australia [*McQueen et al.*, 1999]. We thank the authors for permission to republish these diagrams.

that the abundance of carbon in BFFCs could be of a sufficient quantity to have relevance to atmospheric CO_2 on a Quaternary timescale.

This research follows in the footsteps of Schlesinger, who three decades ago first estimated the pool of carbon stored in the carbonate of desert soils using data from 91 Arizona soils, concluding that "accumulations of pedogenic carbonate in desert soils endow these regions with a greater importance in the global carbon cycle than the amount of soil organic matter, biomass, and proportional land area would otherwise suggest" [*Schlesinger*, 1982, p. 253]. For the sake of making an initial estimate, *Schlesinger* [1982, p. 253] "assume(d) that the area of Arizona is representative of the diversity of landscapes and soils characteristics of arid and semiarid regions of the world." Schlesinger's findings were then replicated in Arizona [*Rasmussen*, 2006] and in Spain [*Diaz-Hernandez*, 2010]. We similarly focus our efforts in Arizona and sites in the adjacent Mojave Desert of California to obtain a first rough understanding of the abundance of carbon stored inside desert bedrock.

2. Recognized Characteristics of Bedrock Fractures Filled With Carbonate

Carbonate accumulates inside bedrock in arid and semiarid environments regardless of the host rock material. BFFCs have been noted occurring in rhyolitic tuff at Yucca Mountain, Nevada, USA [*Denniston et al.*, 1997; *Wilson et al.*, 2003], sandstone in Utah, USA [*Heilweil et al.*, 2007], granite in Spain [*Chiquet et al.*, 1999], gneiss in India [*Durand et al.*, 2006], different metamorphic and crystalline rocks in Australia [*McQueen et al.*, 1999;

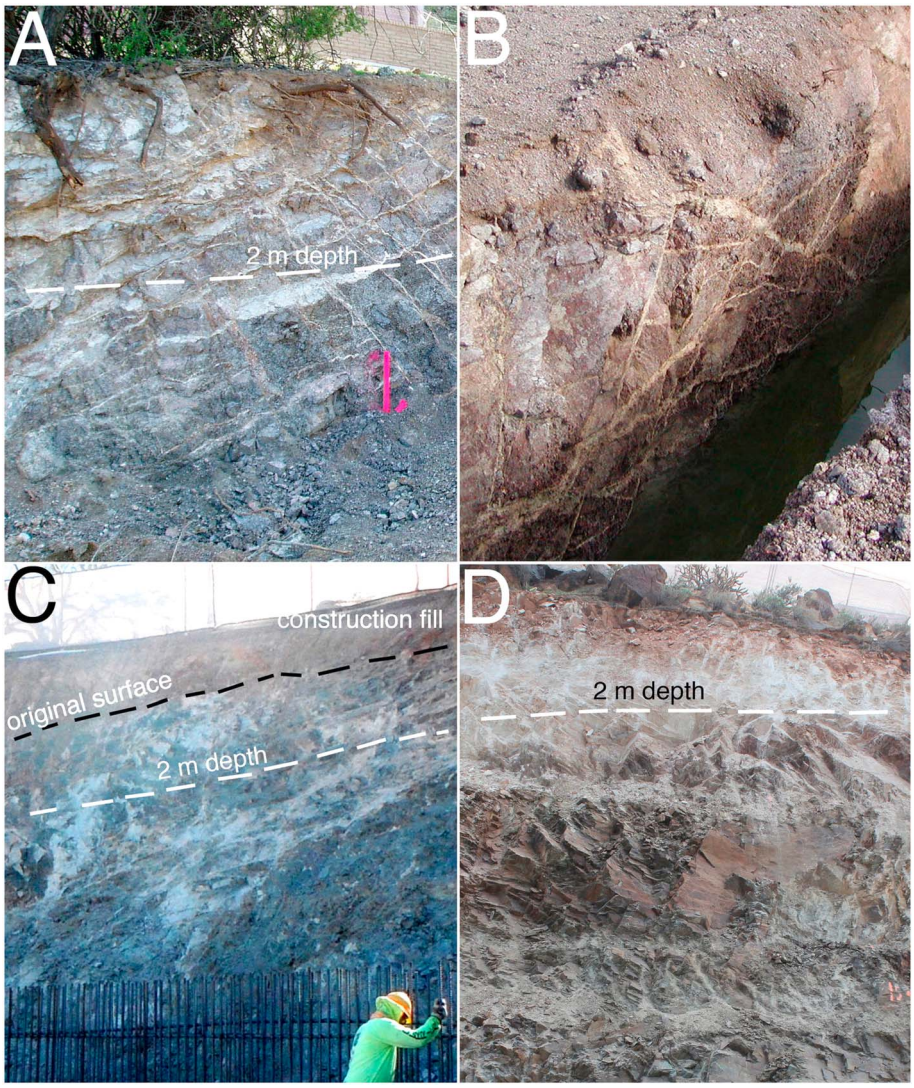

Figure 2. Views of bedrock fractures filled with carbonate exposed in metropolitan Phoenix, Sonoran Desert, Arizona: (a) orthogonal carbonate fills in diorite joints exposed in a 4 m house construction cut; (b) white carbonate fills exposed in a 3 m deep trench excavated to lay pipes; the landform is a granodiorite pediment 2.5 km distant from the adjoining range; (c) construction of a fire station water tank exposure of carbonate veins in gneiss foliations; (d) home construction exposed carbonate veins penetrating into metasedimentary rock. While most of the carbonate found in bedrock fractures occurs in the upper 2 m, penetrations can exceed 10 m.

Quade et al., 1995], and basalt in Hawaii [*Capo et al.*, 2000], Arizona [*Knauth et al.*, 2003], and Morocco [*Hamidi et al.*, 1999, 2001]. While it is certainly possible that some of the carbonate fill studied previously (Figure 1) could have derived, in some part, from burial history [*Winter and Knauth*, 1992], the clear reduction in carbonate abundance with depth (Figures 1 and 2) likely reflects a distance decay from a surficial source of transporting meteoric fluids [*Chiquet et al.*, 1999; *Durand et al.*, 2006; *Hamidi et al.*, 1999; *Heilweil et al.*, 2007; *Knauth et al.*, 2003].

The most detailed research on carbonate veins relates to deposits at Yucca Mountain, Nevada, with the premise that the carbonate informs on paleohydrological conditions [*Carlos et al.*, 1993]. Drill core excavations exposed calcite deposits at depths as great as 500 m infilling open or closed fractures, cementing breccia zones, and penetrating portions of porous tuff [*Vaniman and Chipera*, 1996]. In the upper ~15 m strontium isotopes [*Peterman et al.*, 1992] and carbon and oxygen isotope analyses [*Whelan and Stuckless*, 1992] indicated surficial sources of pedogenic carbonate. *Whelan et al.* [1994] obtained ^{14}C ages of 21–45 ka on 11 samples of calcite from this upper zone, and three samples with indefinite ages. *Szabo and Kyser* [1990] inferred episodic

calcite deposition events at 28 ka, 170 ka, and 280 ka using U-series dating. In lower stratigraphic zones, the crystal morphology of the calcites has been documented to shift from a fine-grained texture to coarser grained, tabular deposits in fractures, or filling voids [*Vaniman and Chipera*, 1996]. Observation that lanthanide enrichment of calcites occurs at greater depths led to the hypothesis that the sources of Ca for the deeper calcites was hydrothermal or related to groundwater upwelling [*Bish and Chipera*, 1989; *Bish and Aronson*, 1993; *Vaniman and Chipera*, 1996], but studies of U, Th, and Pb isotopes [*Neymark et al*., 2002; *Szabo and Kyser*, 1990] and C, O, and Sr isotopes [*Neymark et al*., 2005; *Whelan et al*., 2002] have been interpreted to indicate deposition by downward percolation of meteoric water [*Stuckless et al*., 1991].

Whether accumulated terrestrial carbonate represents bedrock weathering or carbonate recycled from other resources has been addressed most often through Sr isotope ratios [*Capo and Chadwick*, 1999; *Chiquet et al*., 1999; *Dart et al*., 2007; *Violette et al*., 2010]. In these studies $^{87}Sr/^{86}Sr$ ratios of groundwater, surface water, parent bedrock material, and eolian dust are measured and compared to the $^{87}Sr/^{86}Sr$ ratios of carbonates. Where the parent material has high calcium content (e.g., basalt) and experiences high weathering rates, in situ weathering appears to be an important input [*Capo et al*., 2000]. In the majority of arid and semiarid environments where Sr has been used to determine the provenance of Ca in carbonate, the Ca appears to be derived from aerosols [*Capo and Chadwick*, 1999; *Chiquet et al*., 1999; *Quade et al*., 1995].

In the Iberian Hercynian Massif of Central Spain, *Chiquet et al*. [1999] analyzed a vertical profile with a continuous calcrete horizon underlain by weathered and fresh granite infused with calcium carbonate. The authors measured Sr isotopes of the carbonate from depths ranging from 0.01 to 3.8 m, as well as in dust on the surface. The $^{87}Sr/^{86}Sr$ in the bedrock is much higher than the values measured in the carbonate accumulation at all depths. The $^{87}Sr/^{86}Sr$ of the surface and groundwater are both within the value range for the $^{87}Sr/^{86}Sr$ of the carbonates, indicating that the primary source of calcium in these carbonate deposits is not weathering of local bedrock. Analyses of carbonates at sites containing BFFCs in Morocco and Australia similarly reveals only minor uptake in CO_2 from bedrock weathering [*Dart et al*., 2007; *Hamidi et al*., 2001]. In contrast, about 55% of the carbonates deposited in the early Holocene and late Pleistocene in southern India derive from local bedrock weathering [*Durand et al*., 2006, 2007; *Violette et al*., 2010].

Despite the diverse interest in BFFCs presented in this brief review, no prior research has attempted to estimate the amount of carbon stored inside the bedrock of mountains and pediments in drylands. The next section presents field and laboratory methods used in our effort to obtain a better understanding of the amount of carbon stored in BFFCs.

3. Methods

To estimate the carbon pool of BFFCs in southwestern desert mountains, we first located excavations. Recent exposures are important, because the friable nature of the carbonate results in flaking that reduces measured values over time. Second, the portion of the cut analyzed was selected through an objective process (see below), so that sampling did not favor exposures either reduced or relatively enriched in BFFCs. Third, we measured the percent C and density of the BFFCs from randomly collected samples in the excavations. Lastly, the C content of samples within sites was converted to a basic unit of mT C/m^2.

In addition to compiling the first estimate of the storage of carbon in desert bedrock, we also conducted backscattered electron (BSE) microscope studies to examine whether BFFCs are stored in fractures smaller than studied through fieldwork. An additional goal of the BSE study was to look for textures that would suggest postdepositional diagenesis [*Bathurst*, 1972; *Chitale*, 1986; *Klappa*, 1979; *Moore*, 1989; *Nash and McLaren*, 2003; *Stokes et al*., 2006; *Verrecchia*, 1990; *Watts*, 1980]. We conducted pilot radiocarbon and Sr isotope analyses in samples where BSE textures did not show evidence of postdepositional diagenesis.

3.1. Measurement of Carbonate Abundance in Excavations

This study pools data from a quarter century of examining excavations made by bulldozers at Sonoran and Mojave Desert sites. These excavations come in all different dimensions (e.g., Figure 2) including small exposures associated with home construction, long and shallow exposures during road construction, and deep excavations for such features as water towers.

A comparison of different sites requires a common depth of measurement. We decided to focus on the upper 2 m for a few reasons. First, many excavations did not go significantly deeper than 2 m, so using this depth

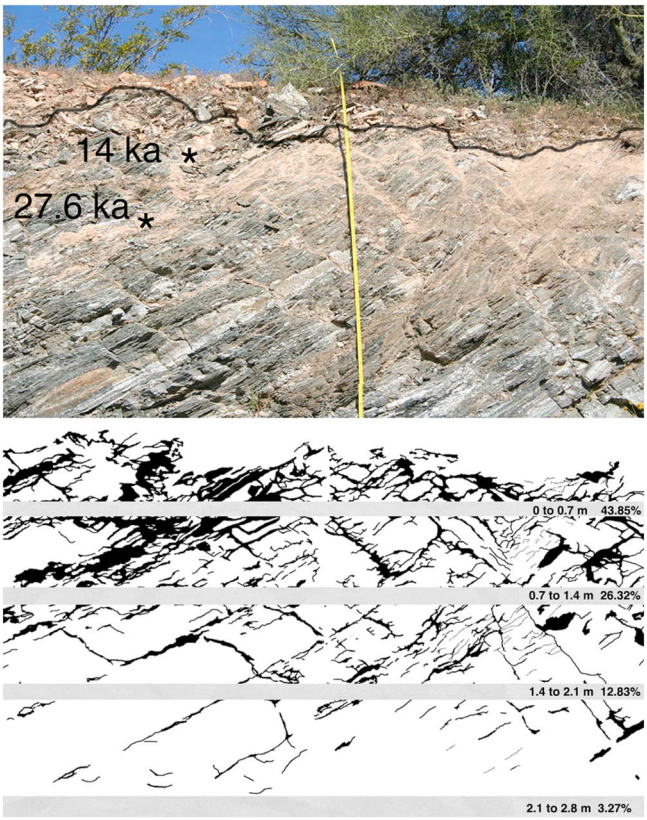

Figure 3. Marketplace road excavation cut into the Gila Range, central Arizona, where digital image processing generated a map of the carbonate veins in bedrock. Asterisks indicate the location of radiocarbon samples collected from a vein. Note the higher cross-sectional area percentages of carbonate closest to the surface. The colluvium and soil are not parts of the carbonate mapping; mapping of the fractures filled with carbonate only occurs in the area of exposed bedrock; the line in the upper photo separates mapped bedrock from unmapped colluvium and soil.

greatly increased the number of excavation sites that could be compared. Second, prior studies have suggested that carbonate contents decline strongly at depths below 2 m [*Chiquet et al*., 1999; *Durand et al*., 2006; *Heilweil et al*., 2007]. We observe this decline at our study sites.

We employed two different strategies to randomize the particular exposure of 20 m^2 analyzed at an excavation, based on the amount of exposed bedrock. In circumstances such as a subdivision with abundant road cuts, a stratified random sampling approach was used to select the study sites. The subdivision was divided into grids, and random number generator was used to select grid squares to be analyzed. Then, within the grid, we selected the bedrock exposure closest to the center point of the grid that adhered to specific criteria: (i) an exposure that has not been obscured by weathered materials or vegetative cover; (ii) a minimum of 2 m in height and 10 m in length; and (iii) safe access. Second, when excavations had more than 20 m^2 of exposure, we analyzed the "cleanest" 20 m^2 of exposed cross section (least vegetation/fill covering, and most planar surface).

We used two approaches to measure the percent of BFFCs found in bedrock fractures. During the early years of data collection for this study, rolls of gridded plastic were pinned to exposures. Markers mapped out BFFCs with widths greater than 3 mm on the grids, that were then counted manually and a percentage calculated for an excavated exposure of 20 m^2. During later years of data collection, we used digital image processing of high-resolution photographs. Carbonate veins were manually mapped as a separate layer in a photo editor. Then, this mapping was rechecked in the field to minimize the chance of mismapping features like igneous veins or quartz-rich foliations as carbonate. After field rechecking, BFFC maps were processed as separate images. This black and white map of BFFC veins enables the calculation of percent area of BFFC with NIH Image software (Figure 3). These manual (27 excavations) and automated (four excavations) procedures generated an overall percent of bedrock occupied by carbonate veins in 31 different locales in the Sonoran and Mojave Deserts, southwestern USA, with coordinates presented in Table 1. We did not test both methods on a single excavation

Table 1. Metric Tons of Carbon Observed at Excavations of Bedrock in the Sonoran and Mojave Desert

Site	Rock (Hillslope or Pediment)	Coordinates	% CaCO3	% C	± SD	g/cm^3 ± SD	mTC/m^2 ± SD
303 Site 1[a]	Basalt (H)	N 33.75193 W 112.29585	20.64	8.04	± 1.58	2.00 ± 0.33	0.066 ± 0.022
303 Site 2[a]	Sandstone & Breccia (H)	N 33.76538 W 112.28804	5.23	7.27	± 1.35	1.92 ± 0.34	0.015 ± 0.005
Adobe Mountain	Basalt (H)	N 33.69376 W 112.11642	38.40	7.97	± 1.62	2.08 ± 0.31	0.127 ± 0.041
Anthem	Metavolcanic (H)	N 33.86550 W 112.09160	12.77	9.43	± 1.79	1.79 ± 0.30	0.043 ± 0.014
Anthem	Metavolcanic (P)	N 33.86550 W 112.09160	19.35	8.85	± 1.51	2.10 ± 0.27	0.072 ± 0.020
El Paso Gas Pipeline Site 1	Metasedimentary (H)	N 33.97452 W 112.13994	14.44	8.79	± 1.41	2.11 ± 0.30	0.054 ± 0.015
El Paso Gas Pipeline Site 2	Granitic (H)	N 34.13584 W 112.15820	23.01	9.07	± 1.24	2.03 ± 0.31	0.085 ± 0.023
El Paso Gas Pipeline Site 3	Basalt (H)	N 34.29871 W 112.17479	37.22	8.33	± 1.49	1.97 ± 0.38	0.122 ± 0.041
Estrella Mountain Ranch	Granitic (H)	N 33.29646 W 112.42709	26.07	9.31	± 0.56	2.04 ± 0.41	0.099 ± 0.025
Estrella Mountain Ranch	Granitic (P)	N 33.29646 W 112.42709	39.55	8.68	± 1.32	1.89 ± 0.34	0.130 ± 0.040
Fountain Hills	Breccia	N 33.58870 W 111.73826	6.65	7.89	± 1.89	1.83 ± 0.29	0.019 ± 0.007
Gila Foothills	Gneiss (H)	N 33.30636 W 112.06145	32.58	8.71	± 1.76	2.45 ± 0.32	0.139 ± 0.043
Gold Canyon 1	Ignimbrite (H)	N 33.37596 W 111.44589	9.44	8.25	± 1.12	2.19 ± 0.28	0.034 ± 0.008
Gold Canyon 2	Ignimbrite (H)	N 33.37059 W 111.45409	13.22	7.88	± 1.69	2.13 ± 0.33	0.044 ± 0.015
Gold Canyon 2	Ignimbrite (H)	N 33.37219 W 111.46714	21.48	8.16	± 1.42	2.06 ± 0.27	0.072 ± 0.020
Golden Eagle 1	Metasedimentary (H)	N 33.63841 W 111.77947	42.06	8.47	± 2.02	1.86 ± 0.28	0.133 ± 0.047
Golden Eagle 2	Metasedimentary (H)	N 33.63888 W 111.77404	17.66	8.90	± 1.16	2.04 ± 0.27	0.064 ± 0.016
Hedgpeth Hills	Basalt (H)	N 33.68186 W 112.17058	37.29	7.95	± 1.92	1.87 ± 0.35	0.111 ± 0.043
Hwy 58 Site 1	Granitic (P)	N 35.01643 W 117.97553	25.03	8.02	± 1.45	1.98 ± 0.35	0.079 ± 0.026
Hwy 58 Site 2	Granitic (P)	N 35.01791 W 118.00115	32.19	8.51	± 1.49	2.05 ± 0.33	0.112 ± 0.035
Las Sendas	Granitic (H)	N 33.48364 W 111.67462	24.06	10.06	± 0.65	1.95 ± 0.34	0.094 ± 0.021
Las Sendas	Granitic (P)	N 33.48462 W 111.67494	35.29	8.46	± 1.25	2.17 ± 0.31	0.130 ± 0.035
Lost Canyon	Metavolcanic (H)	N 33.69334 W 111.85147	16.37	7.32	± 1.38	2.02 ± 0.31	0.048 ± 0.015
San Tan Site 4	Metasedimentary (H)	N 33.19670 W 111.64982	18.78	8.05	± 0.95	2.11 ± 0.36	0.064 ± 0.017
San Tan Site 1	Granitic (H)	N 33.15223 W 111.61566	18.65	8.40	± 1.47	2.08 ± 0.28	0.065 ± 0.019
San Tan Site 2	Granitic (P)	N 33.16001 W 111.62084	22.56	7.90	± 1.66	2.20 ± 0.20	0.078 ± 0.022
San Tan Site 3[a]	Sandstone (H)	N 33.11868 W 111.64126	6.41	8.41	± 1.71	2.22 ± 0.36	0.024 ± 0.008
Scottsdale Mountain	Metasedimentary (H)	N 33.60866 W 111.78678	14.00	7.96	± 1.42	2.05 ± 0.38	0.046 ± 0.015
Stetson Hills[a]	Basalt (H)	N 33.72153 W 112.14762	34.91	8.51	± 1.46	1.98 ± 0.28	0.118 ± 0.034
Verado	Granitic (H)	N 33.48444 W 112.51255	20.55	8.16	± 0.90	2.13 ± 0.27	0.071 ± 0.016
Verado	Granitic (P)	N 33.48444 W 112.51255	36.11	8.70	± 1.08	1.67 ± 0.40	0.105 ± 0.035

[a]Vertical cross sections were not available. At these sites, construction activity exposed bedrock parallel to the former surface. These study locations occur 0.5 m beneath the former bedrock hillslope surface.

because of the lapse in time between the application of the analogue method and the digital approach. The results of digitally remapping an exposure initially recorded with the analogue method would not be possible because of friable/erodible nature of exposed carbonate veins documented in the resampling study done at the Golden Eagle excavation, presented in section 4.3.

Since bulldozers do not generate cubes, the assumption made for each site is that 2-D percentages acquired for an excavation are valid approximates for 3-D percentages of carbonate infused into bedrock. We were able to assess the periphery of 3-D blocks assumption at three different sites where a bedrock excavation made turns approximating a right angle: Scottsdale Mountain, Golden Eagle 2, and Las Sendas sites in Table 1. At these locations three sides of a rectangular solid were analyzed for the percent carbonate exposed in a cross section.

Carbonate deposited inside bedrock fractures can be quite friable. While we made every attempt to collect data from sites recently dynamited or bulldozed, some sites were not identified until years after excavation. Thus, to understand if abundances would decrease over time in an exposure and bias findings, we returned to four exposures (Golden Eagle 1, Golden Eagle 2, Gold Canyon 1, and Gold Canyon 2) years after the initial study of a site. The return visit then led to a new measurement of the percent of exposed carbonate and a better understanding of how the abundance in a bedrock exposure can change over time.

3.2. Measurement of Percent Carbon and Sample Density

Ten samples were collected from each exposure, typically along two veins at depths of 0.4, 0.8, 1.2, 1.6, and 2.0 m. These samples were split for analysis of the percent carbon and the sample density. The samples were analyzed at the Goldwater Environmental Laboratories at Arizona State University by a Perkin-Elmer elemental analyzer to determine the weight percent carbon. Density (g/cm^3) was measured by determining the volume of weighed sample from the displacement of water in graduated cylinders.

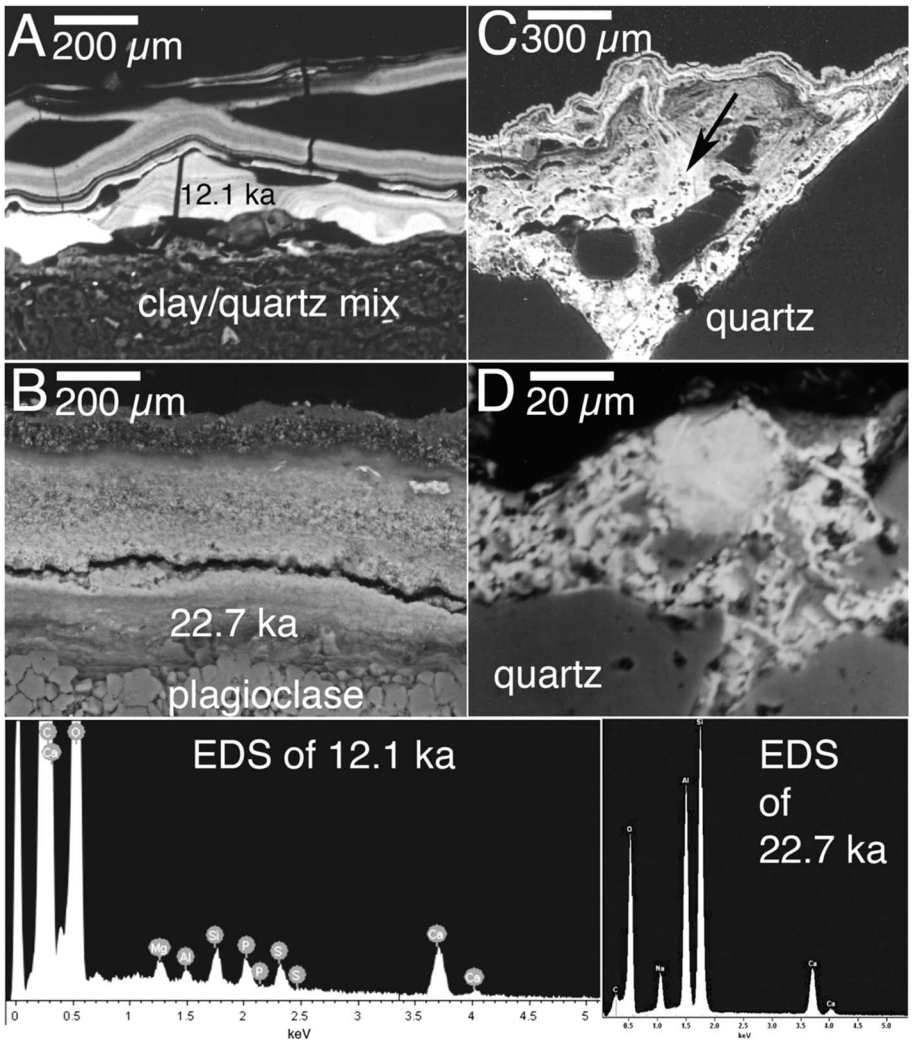

Figure 4. BSE imagery of laminar textures used in (a and b) ^{14}C and (c and d) nonlaminated textures avoided for ^{14}C dating (see Figure 4 for field context). The laminar texture in Figure 4a separated nicely from the weathered sidewall of the fracture and from the overlying silica-rich (darker) layer in sample scraping with a tungsten-carbide needle. The dated laminar texture in Figure 4b is darker than the overlying granular layer, because it contains some clay minerals (Na, Al, and Si in the EDS spectra). The overlying granular layer had to be physically abraded away with a Dremel drill to separate it from the underlying laminar texture. We explicitly avoided textures showing remobilization of carbonate (e.g., arrow in Figure 4c showing cross-cutting reprecipitation) and mixed textures of silica and carbonate (Figure 4d) suggestive of ongoing diagenesis through silica substitution.

3.3. Calculation of Carbon Abundance

For each site in Table 1, the quantity of C per square meter of surface to a depth of 2 m was calculated as follows:

$$C/m^2 = bvCD \quad (1)$$

where b is the percent of bedrock fracture fills composed of calcium carbonate in the upper 2 m of a bedrock exposure, v is the volume in cm^3 of a rectangular solid that is 2 m deep with a surface area of $1\,m^2$, or $2 \times 10^6\,cm^3$, C is the carbon content of the BFFCs at a site, measured in percent C by weight, and D is density of the BFFCs

Quantities of carbon were reported as mTC/m^2.

The standard deviations of the percent C and density propagates into the error term of mTC/m^2 for each site. One standard deviation of the average of percent C and density generates the reported standard deviation of mTC/m^2 using equation (1).

3.4. Electron Microscope Analysis

Backscattered electron (BSE) microscopy generates gray scale images of average Z from polished cross sections. Bright portions of the image reflect a higher atomic number [*Krinsley and Manley*, 1989]. Energy dispersive X-ray spectrometry (EDS) provides elemental data of the different micron-scale areas visualized through the BSE detector [*Goldstein et al*., 2003]. We employed BSE and EDS in three separate investigations.

The field-based methods used to measure carbon abundance at sites in Table 1 only analyze veins of carbonate wider than 3 mm. This means that all veins smaller than 3 mm are not included in the reported values. To investigate the possibility that carbonate infuses into bedrock in submillimeter veins, samples of bedrock without any visually apparent carbonate veins were collected from depths of 0.2, 0.4, 0.6, 0.8, 1.0, 1.2, 1.4, 1.6, 1.8, and 2.0 m from the Las Sendas site imaged in Figure 2a. Then, for each sample, a cross-sectional area of 1.0 mm^2 was polished and analyzed through acquisition of multiple images at a magnification of 1000 times; EDS was employed to identify carbonate. Then, digital image processing quantified the percent carbonate at each of these depths, using methods described elsewhere [*Dorn*, 1995]. This approach generates a profile of changes in percent carbonate with depth in samples that had no visually apparent presence of a BFFC.

The second use of BSE and EDS involved a qualitative study of BSE textures of the BFFC samples. One sample from a depth of 1 m in one vein from each site in Table 1 was turned into a polished cross section. Textures indicative of postdepositional diagenesis were observed in several samples Figure 4. The third use of BSE relates to the next section on radiocarbon dating.

3.5. Radiocarbon Dating

Soil carbonate is fraught with uncertainties in obtaining reliable ^{14}C results with postdepositional diagenesis a key concern [*Callen et al*., 1983; *Stadelman*, 1994; *Wang et al*., 1994]. The apparent ^{14}C age could be altered when small amounts of capillary water remobilize carbonate. Thus, because it is essential to recognize different carbonate fractions [*Candy et al*., 2003; *Fletcher et al*., 2011] we worked with samples that reflect the initial deposition of laminar calcrete.

In a pilot study, we collected two samples for radiocarbon dating from the Gila Range site in Figure 3. The samples were collected from the same vein at depths of 0.4 m and 0.8 m. BSE was used to identify portions of the samples that had a laminar texture (Figure 4). The laminar carbonate was submitted to Beta Analytic for conventional radiocarbon dating.

3.6. Strontium Isotope Analysis

In a pilot study, we measured $^{87}Sr/^{86}Sr$ isotopic ratios at depths of 1 m, 2 m, and 3 m from the road cut in Figure 3. We analyzed three different types of samples: (i) gneiss bedrock at the surface of excavations, adjacent to the carbonate veins; this gneiss was leached in HCl prior to analysis to remove BFFC carbonate that could modify the Sr signature of the gneiss; (ii) carbonate veins that infill bedrock; samples of this carbonate were collected after removing 30 cm of bedrock; digging back 30 cm minimizes the potential for contamination; and (iii) the leachate solution removed from the gneiss with HCl; because the surface of the gneiss is exposed, this leachate represents carbonate eolian dust that infused into the fractures of the gneiss and likely mixes dust infused before and after the road cut was created.

Concentrations were measured with a Thermo Neptune MC-ICP-MS. Two standards were run in triplicate: SRM987 at 0.710259 ± 0.000013 compared to the standard range of 0.71022–0.71030; and the U.S. Geological Survey standard G-2 at 0.709836 ± 0.000008 compared to 0.70983 [*Balcaen et al*., 2005]. During the run, standard SRM987 was run with a measured $^{87}Sr/^{86}Sr$ value of 0.710266 ± 0.000032 (2 standard deviation) or ±0.000003 (1 SE; n = 26). For external reproducibility, we ran one of the samples in three replicates with a mean and 1 standard deviation of 0.705482 ± 0.000028.

4. Results

4.1. Abundance of Carbon at Sonoran and Mojave Desert Excavation Sites

Values of mTC/m^2 were calculated for the upper two m of 31 excavations in the Sonoran and Mojave Deserts. The sites consist of different rock types, ranging from basalt to sandstone. Locations include 24 excavations into bedrock hillslopes and seven excavations of bedrock pediments. The percent of the excavation area

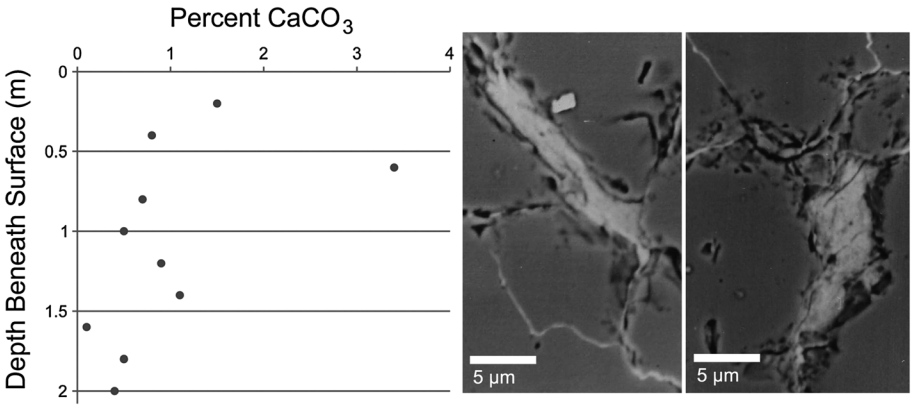

Figure 5. Percent calcium carbonate in micron-scale veins at the Las Sendas site. Each value on the graph represents the cumulative calculation of veins in an area of about 1 mm^2. The two BSE images show typical views of the carbonate found in micron-scale veins in samples that showed no visual evidence of impregnation with calcium carbonate.

consisting of calcium carbonate veins averaged 23.3% (range 5.2% to 42%) (Table 1). The percent carbon averaged 8.4% (range 7.3%–10%), consistently less than the expected value of 12% for calcite (Table 1). The density of the samples averaged 2 g/cm^3 (range 1.7–2.4), less than the expectation for calcite of 2.71 g/cm^3 (Table 1). The total mass of carbon in these desert mountains averaged 0.079 mTC/m^2, ranging from 0.015 to 0.139 (Table 1). Each site in Table 1 has an error for the mTC/m^2 stored in the upper 2 m. This site-specific error incorporates the 2σ errors in the C and density measurements. The site-specific values then lead to the calculation of a standard deviation of ± 0.036 mTC/m^2 for the 31 evaluated exposures.

4.2. Variation in Three Sides of an Exposure

The assumption that 2-D excavations generate similar abundances of carbon as 3-D rectangular blocks was assessed at three different sites in Table 1. At Scottsdale Mountain, sides 1, 2, and 3 of a rectangular solid displayed carbonate abundances of 12.35%, 13.70%, and 15.95%, respectively. At Golden Eagle Site 2, sides 1, 2, and 3 of a rectangular solid displayed abundances of carbonate of 18.69%, 15.04%, and 19.25%, respectively. At Las Sendas, sides 1, 2, and 3 of a rectangular solid displayed abundances of carbonate of 21.55%, 24.51%, and 26.04%, respectively. These measurements, while not statistically significant, provide an idea of the variability seen around the margins of some 3-D blocks.

4.3. Carbonate Erosion From Excavations

Our repeated measurements over time reveal that carbonate content of faces declines strongly with time after excavation. Golden Eagle sites 1 and 2 were revisited 1, 2, and 3 years after the initial study of an excavation analyzed within a week of bulldozing. The percent carbonate declined from 42.06% to 33.19% in 3 years at Golden Eagle 1. At Golden Eagle 2, the decline was from 17.66% to 3.88%.

Gold Canyon sites 1 and 2 were revisited 5 and 10 years after the initial study of an excavation that was studied 2 years after construction. The percent carbonate at Gold Canyon 1 declined from 9.44% to 1.81% 5 years later and down to 0.50% 10 years after the first measurement. At Gold Canyon 2, 13.22% declined to 5.05% after 5 years and to 1.20% after 10 years.

4.4. Abundance of Carbonate in Microveins

A BSE investigation of micrometer-scale fractures at the Las Sendas site (Figure 2a and Table 1) reveals that calcium carbonate comprised about 1% of rock area (Figure 5). These samples showed no visual evidence of BFFC penetration when collected in the field. At this site, the abundance of micron-scale carbonate also declined with depth.

4.5. BSE Carbonate Textures

The qualitative investigation of the carbonate veins using BSE to image samples collected at depth of a meter from each site revealed a wide range of textures. Figure 6 presents a few of the observed textures that include evidence of ongoing silica substitution for carbonate (Figures 6a and 6b), the encapsulation of silicate silt by

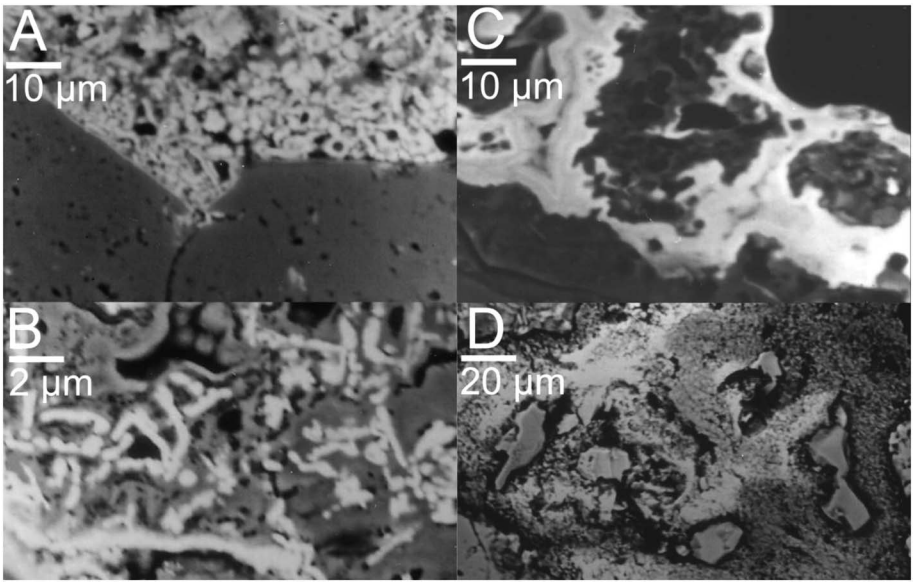

Figure 6. BSE imagery of BFFCs show evidence of silica replacement, from the site in Figure 3. (a) The carbonate (bright, higher Z) adjacent to quartz (darker gray scale, lower Z). The brighter carbonate has a granular texture that is mixed with darker areas of silica indicative of postdepositional replacement of carbonate [*Watts*, 1980], documented through EDS analyses. Note the pores in the quartz. We speculate that silica mobilized from the quartz is substituting for the carbonate with ongoing movement of capillary water. (b) A mixing of silica (darker areas) and carbonate (brighter granular linear features). We interpret this texture as calcium carbonate being replaced with silica. (c) Silt-sized silicate particles (darker) that appear to be encapsulated by carbonate (bright); the quartz wall of the vein is in the lower left. (d) A transition from less porous (lighter) carbonate on the left to more porous carbonate on the right. Silt fragments of quartz intermix with the carbonate.

laminar calcrete (Figure 6c), and granular-textured carbonate with considerable variability in porosity (Figure 6d)—a texture observed elsewhere in field studies [*Durand et al*., 2007].

The BSE imagery in Figures 4–6 explains why percents of carbon in these veins were considerably less than the theoretical value of 12% for $CaCO_3$ and why densities tended to be lower than the expected 2.71 g/cm^{-3} for calcite. BSE images reveal that detrital pieces of quartz and other silicates cooccur with carbonate in the veins. Also, silica substitution of carbonate occurs to varying degrees at different sites.

4.6. Radiocarbon Results

Two pilot samples analyzed for radiocarbon dating provide evidence for carbonate mobility in the last glacial period. Samples collected at depths of 0.4 m and 0.8 m in a carbonate vein in the Gila Range excavation (Figure 3) revealed the following:

$$\text{At } 0.4 \text{ m depth : } 12120 \pm 50 \text{ BP } (\text{Beta } 322776)\,{}^{13}C/{}^{12}C - 5.9 \text{ o/oo}$$

$$\text{At } 0.8 \text{ m depth : } 22680 \pm 90 \text{ BP } (\text{Beta } 322775)\,{}^{13}C/{}^{12}C - 9.2 \text{ o/oo}$$

These radiocarbon measurements have calibrated ages with 2σ error of Cal BP 14050-13850 (intercept Cal BP 13970) and Cal BP 27780-26980 (intercept Cal BP 27640), respectively [*Heaton et al*., 2009].

These data suggest that the carbonate precipitated when the Sonoran Desert around this site hosted a pygmy conifer woodland [*Allen et al*., 1998; *McAuliffe and Van Devender*, 1998; *Van Devender et al*., 1987]. It is conceivable that a pulse of intense wetness resulted in the transport and precipitation of the dated laminar carbonate (Figure 4) to depths of 0.4 and 0.8 m. An alternative interpretation is that water moved along the sidewalls of the vein and simply remobilized and reprecipitated preexisting carbonate that was initially deposited long before the last glacial period. Either explanation would require that the depth of water penetration into these fractures would be deeper than that exists at the present time.

4.7. Strontium Isotope Results

The $^{87}Sr/^{86}Sr$ ratios for pilot samples collected from the Marketplace road cut (see Figure 3) in Table 2 compares three types of samples collected from depths of 1 m, 2 m, and 3 m. The $^{87}Sr/^{86}Sr$ ratios of the BFFC

Table 2. Pilot Strontium Isotope Results from the Marketplace Road Cut (See Figure 3)

Depth	Gneiss $^{87}Sr/^{86}Sr$	Carbonate Vein $^{87}Sr/^{86}Sr$	Dust Leachate $^{87}Sr/^{86}Sr$
1 m	0.705482	0.709901	0.710015
2 m	0.706099	0.710620	0.711143
3 m	0.724398	0.710435	0.710064

rest between the gneiss and the dust leachate at all depths. However, the $^{87}Sr/^{86}Sr$ ratios of the fracture-fill carbonates appear to be more similar to the dust leachate than the gneiss.

These findings parallel results presented by *Naiman et al*. [2000] in a study that sampled soil carbonate and carbonate rinds on boulders in a 150 km radius of Tuscon, Arizona; the $^{87}Sr/^{86}Sr$ ratios of patent materials ranged from (0.7029 to 1.88), dust samples ranged from (0.7100 to 0.7123), and soil carbonates ranged from (0.7049 to 0.7190). In all cases *Naiman et al*. [2000] found that soil carbonates derived from a combination of weathered parent material and dust, with relative percentages of contribution being dependent on the nature of the parent material.

5. Discussion

5.1. Assessing Bias in Observed Values of Stored Carbon

There are three reasons that the mTC/m^2 amounts reported in Table 1 are likely minimum values for each of the study sites. First, BFFCs continue into bedrock fractures deeper than the 2 m analyzed here (e.g., Figures 2 and 3). Second, the BFFCs are often quite friable and erode over time, as indicated by the revisitation analysis presented in section 4.3. The third reason our reported values would be minimums is that BFFCs exist at a variety of scales—from veins many centimeters wide down to micrometer widths. Since the methods we used here only mapped veins thicker than about 3 mm, BFFCs in the thinnest veins are not included in Table 1. The BSE study of one site reported in section 4.4 suggests that micron-scale veins represented about 1% of the rock volume. Thus, it is likely that the observed mTC/m^2 values for studied sites in Table 1 are minimum estimates.

5.2. Potential Size of the BFFC Carbon Reservoir

For the sake of assessing the potential significance of the global BFFC carbon pool we calculated the size of the global pool that could potentially exist if other arid and semiarid regions have similar BFFC carbon content as our study sites. While we acknowledge this assumption could be incorrect, the Mojave and Sonoran deserts reflect a mix of bedrock types (Table 1) and include cold-season and bimodal precipitation regimes. Thus, we carry out this potential carbon pool estimate as an intellectual exercise to be revised as more data become available.

Meigs [1953] calculated that the world's arid and semiarid deserts consist of 46.7 million km^2 or 4.67×10^{13} m^2. *Goudie* [2003] tabulates that desert mountains occupy 38%, 43%, 39%, and 47% of the southwestern USA, Saharan, Libyan, and Arabian deserts. *Hurley et al*. [2004] present values for bedrock highlands of 47%, 43%, and 16% for the Arabian, Saharan, and Australian warm deserts. The area of each of these deserts was multiplied by the percent of bedrock highlights in each desert—resulting in an approximate figure of 40% of arid and semiarid regions occupied by mountain ranges or 1.87×10^{13} m^2.

Multiplying 0.079 mTC/m^2 (Table 1) by 1.87×10^{13} m^2 suggests the possibility that there could potentially be 1485 GtC of stored carbon in the upper 2 m of desert mountains. This speculative value is roughly similar to the world's pool of soil organic carbon (1600 GtC) or pool of pedogenic carbonate (780–940 GtC) [*Eswaran et al*., 1993, 1999; *Falkowski et al*., 2007; *Lal*, 2004, 2008; *Schlesinger*, 1982; *Sundquist*, 1993].

There are four reasons the estimate of 1485 GtC could be a minimum. First, there is a substantive difference between the estimated planimetric area of desert mountains [*Goudie*, 2003; *Hurley et al*., 2004] and the much larger surface area of mountain slopes. Second, hyperarid deserts could potentially contain BFFCs. The second author observed two metasedimentary rock excavations containing 4–6% BFFCs in southern coastal Peru. However, hyperarid mountains are not included in our calculations, because the age of the cuts were unknown and two sites do not justify including hyperarid mountains in a global estimate. Third, bedrock pediments are relatively flat landforms [*Dohrenwend and Parsons*, 2009] and are not included in estimates of

Table 3. Compilation of Bedrock and Pediment Erosion Rates in Arid Lands

Study	Location	Bedrock Erosion Rate
Kounov et al. [2007]	South African escarpment	1.5–3 mm/ka
Bierman and Caffee [2001]	Namib Desert	1.1–7.5 mm/ka
Nichols et al. [2005]	Mojave Desert	21–100 mm/ka
Hunt and Wu [2004]	Mojave Desert	31 mm/ka
Heimsath et al. [2006a, 2006b]	Southeastern Australia	9 mm/ka and 22 mm/ka
Decker et al. [2011]	South Africa	2.5 mm/ka

the area of deserts occupied by mountains, because geomorphologists do not consider pediments to be mountains. However, for the purposes of estimating this carbon pool, pediments certainly add to the total area of bedrock-atmosphere interface. We are unaware of a reasonable estimate for the area of arid bedrock pediments globally. Thus, adding in the area of pediments would increase the global estimate of carbon in the BFFC pool. Fourth, section 5.1 details why the 0.079 mTC/m^2 values for the studied sites is likely a minimum.

There are also reasons the approximately 1485 GtC estimate could be too high. First, the Sonoran and Mojave sites are dominated by plutonic and metamorphic lithologies, rather than sedimentary or extrusive rock types, and it is possible that the fracture density at the studied excavations could enhance carbonate penetration into bedrock. Second, the studied sites are located mostly in arid environments and a better representation of semiarid sites could reveal a lower abundance of carbonate. Third, the studied sites are located in settings that have experienced subsurface rock decay prior to subaerial exposure; it is possible that this "preweathered" state could enhance BFFC penetration. Fourth, the area of carbonate mountain ranges would have to be subtracted if additional studies reveal that the BFFCs in limestone and dolomite derive from the remobilization from fracture walls. Fifth, the studied sites are located in settings that experience dust storms that contain carbonate dust; it is possible that locales experiencing fewer dust storms would host lower values of BFFCs.

5.3. Evaluating the Mass Balance of BFFCs

In our conceptual thinking, the mass of BFFCs is a balance of carbonate insertion into the fractures by precipitation and removal by erosion of the bedrock surface. During the Holocene the southwestern United States has maintained consistently low levels of precipitation. The radiocarbon date obtained on an upper BFFC horizon at 0.4 m would suggest that BFFCs at this Sonoran Desert site did not experience a depth of water penetration in this fracture to 0.4 m in the past ~14,000 years. The ^{14}C ages we obtained are in the range of those obtained by *Whelan et al.* [1994] of 21–45 ka from the upper carbonate veins at Yucca Mountain.

We speculate that BFFCs mass balance has probably experienced a net loss over the arid Holocene period because percolation into deep subsurface fractures likely depends on high levels of precipitation. While further radiocarbon dating of upper BFFC surfaces at other sites could reveal more recent deposition, available data suggest that carbonates in the BFFCs could relate to time periods wet enough to facilitate water penetration into bedrock fractures. Unlike shallow soil systems that are reactive on centennial timescales [*Machette*, 1985; *Monger and Gallegos*, 2000], we speculate that deeper deposits could be relics of particularly intense wet Pleistocene periods.

To estimate the average rate of release of carbonate from bedrock through mechanical erosion, we turn to six studies that present rates of erosion of bedrock and of pediments in arid regions [*Bierman and Caffee*, 2001; *Decker et al*., 2011; *Heimsath et al*., 2001; *Hunt and Wu*, 2004; *Kounov et al*., 2007; *Nichols et al*., 2005]; these studies report rates of erosion ranging from 1.1–9.5 mm/ka in bedrock to 22–100 mm/ka for pediments. Based on the speculative estimate of ~1485 GtC stored in BFFCs in the upper 2 m, the upper millimeter of the bedrock horizon could contain ~0.74 GtC, although this value is probably higher because carbonate concentration tends to decrease with depth. Based on the erosion rates estimated for desert bedrock (Table 3), incremental erosion of bedrock has stripped and exposed a maximum of 7.03 GtC and a minimum 0.81 GtC over the past ka. On pediment slopes reported erosion rates indicate a maximum of 74 GtC/ka and a minimum of 16.28 GtC/ka could have been released by weathering and erosion of BFFCs. The range for

pediment systems is greater than for bedrock masses because of a range of factors that influence these bedrock platforms [*Dohrenwend and Parsons*, 2009].

If periods of aridity are associated with the net release of carbonate trapped in bedrock fractures by mechanical erosion, consider an erosion rate of 4.1 mm/ka (the average of bedrock erosion rates in Table 3, excluding pediment erosion rates). Erosion during the past millennia could have released ~3 GtC from the BFFC reservoir. In this scenario, the weathered carbonate could release ~0.3 GtC per 100 years, representing roughly 0.00004% of the annual carbon flux from terrestrial environments to the atmosphere [*Falkowski et al*., 2007].

5.4. The Carbonate-Silicate Geochemical Cycle

Silicate and carbonate weathering and precipitation are linked in the carbonate-silicate geochemical cycle. Weathering of Ca-bearing silicates leads to the precipitation of pedogenic carbonates through the *Urey* [1952] reaction discussed previously. This process draws down atmospheric CO_2 emplacing the carbon in a continental buffer reservoir. Eventually, carbonate compounds created by this reaction are dissolved and transferred to oceans by river systems, increasing the alkalinity and calcium content of oceans and returning CO_2 to the atmosphere.

Carbonate minerals may be the product of silicate mineral weathering, limestone, or remobilized former pedogenic carbonate. Only in the case of the weathering of silicate minerals does the process of forming carbonate minerals sequester CO_2 from the atmosphere. The weathering of carbonate minerals also removes some atmospheric CO_2, where dissolution of carbonate in water leads to the production of bicarbonate and calcium [*Berner*, 1983]. This impact on atmospheric CO_2 levels is comparatively less than the weathering of silicate minerals because the relatively fast kinetics of carbonate weathering returns CO_2 to the atmosphere rapidly.

Carbonate dissolution and reprecipitation is a more important mechanism in the formation of pedogenic carbonate on short timescales than the weathering of silicate minerals. Recent research presented by *Liu et al*. [2010, 2011] challenged the predominant thought that silicate weathering is the principal regulator of atmospheric carbon over geologic timescales, suggesting a role for carbonate weathering in the drawdown and sequestration of carbon. The weathering of carbonate minerals increases alkalinity in the water cycle and increases the CO_2 content in local water systems [*Liu et al*., 2010, 2011]. Once here, natural aquatic ecosystems uptake weathering-related dissolved inorganic carbon by photosynthesis; the resulting organic carbon is diverted into the lithosphere by sedimentation and burial in a process described as the "biological carbon pump." This questions the long-standing viewpoint that only the chemical weathering of Ca-silicate rocks controls long-term climate change. The claims made by *Liu et al*. [2010, 2011] are that carbonate weathering constitutes 94% of the atmospheric CO_2 sink, compared to 6% for silicate weathering. This research remains controversial in terms of whether carbonate weathering has a geological impact on CO_2 [*Kump et al*., 2000]; the quantity of the impact [*Blum et al*., 1998; *Cao et al*., 2011; *Quade et al*., 2003]; time scale of impact [*Tipper et al*., 2006; *Curl*, 2012]; the role of anthropogenic and natural environmental change [*Zhang*, 2011; *Cao et al*., 2012; *Yang et al*., 2012]; the role of land surface age [*Jacobson et al*., 2002a]; and the influence of microbes [*Lian et al*., 2011].

The results of our pilot investigation presented in Table 2 of $^{87}Sr/^{86}Sr$ ratios of carbonates infilling fractures in one desert pediment suggest that BFFC carbonates appear to consist of mostly recycled dust. Thus, in the classic theoretical framework of silicate weathering-related pedogenic carbonates versus carbonate weathering-related pedogenic carbonates, BFFCs may have little impact on the global carbon cycle beyond extending the length of time that pedogenic carbonate exists in its terrestrial buffer reservoir. However, our study has revealed a significant quantity of carbon is stored in BFFC deposits; and in light of the work of *Liu et al*. [2010, 2011], BFFCs could potentially be remobilized have relevance to the global carbon cycle.

6. Conclusions

Modern excavations of Earth's bedrock skin reveal that carbonate infills bedrock fractures. Measurements in the Sonoran and Mojave Deserts reveal that arid and semiarid mountain ranges and their bounding pediments could be storing a significant quantity of carbon; 31 sites averaged 0.079 ± 0.036 mTC/m^2 in the upper 2 m. Pilot ^{14}C and $^{87}Sr/^{86}Sr$ data from one site are consistent with the hypothesis that recycled carbonate dust infilled a bedrock fracture during the last glacial period, which is known to be a substantially wetter time than the Holocene.

Acknowledgments
This research was supported by the Matthew Bailey Scholarship Award to E.H. and two sabbatical awards to R.D. However, most of the cost of this research has been covered by the companies paying for excavations supporting urban sprawl in southwestern USA deserts. Special thanks are due to the W.M. Keck Foundation Laboratory for Environmental Biogeochemistry at Arizona State University and to Gwyneth Gordon.

References

Allen, C., T. Swetnam, and J. Betancourt (1998), Landscape changes in the southwestern United States: Techniques, long-term data sets, and trends, in *Perspectives on the Land Use History of North America: A Context for Understanding Our Changing Environment*, U.S. Geological Survey Biological Resources Division, Biological Science Report USGS/BRD/BSR-1998-0003. See also http://biology.usgs.gov/luhna/chap9.html, edited by T. D. Sisk, p. 104, U.S. Geological Survey, Reston.

Amundson, R. G., D. D. Richter, G. S. Humphreys, E. G. Jobbagy, and J. Gaillardet (2007), Coupling between biota and Earth materials in the critical zone, *Elements*, *3*, 327–332.

Balcaen, L., I. De Schrijver, L. Moens, and F. Vanhaecke (2005), Determination of the $^{87}Sr/^{86}Sr$ isotope ratio in USGS silicate reference materials by multi-collector ICP-mass spectrometry, *Int. J. Mass Spectrom.*, *242*, 251–255.

Bathurst, R. G. C. (1972), *Carbonate Sediments and Their Diagenesis*, pp. 620, Elsevier, Amsterdam.

Berner, R. A. (1983), The carbonate-silicate geochemical cycle and its effect on atmospheric carbon dioxide over the past 100 million years, *Am. J. Sci.*, *283*, 641–683.

Bierman, P. R., and M. Caffee (2001), Slow rates of rock surface erosion and sediment production across the Namib desert and escarpment, southern Africa, *Am. J. Sci.*, *301*, 326–358.

Bish, D. L., and J. L. Aronson (1993), Paleogeothermal and paleohydrologic conditions in silicic tuff from Yucca Mountain, Nevada, *Clays Clay Miner.*, *41*(2), 148–161.

Bish, D. L., and S. J. Chipera (1989), Revised mineralogic summary of Yucca Mountain, Nevada *Rep. LA–11497-MS*, Los Alamos National Lab, N. M.

Blum, J. D., C. A. Gazis, A. D. Jacobson, and C. P. Chamberlain (1998), Carbonate versus silicate weathering in the Raikot watershed within the High Himalayan crystalline series, *Geology*, *26*, 411–414.

Brantley, S., M. B. Goldhaber, and K. V. Ragnarsdottir (2007), Crossing disciplines and scales to understand the critical zone, *Elements*, *3*, 307–314.

Callen, R. A., R. J. Wasson, and R. Gillespie (1983), Reliability of radiocarbon dating of pedogenic carbonate in the Australian arid zone, *Sediment. Geol.*, *35*, 1–14.

Candy, I., S. Black, B. W. Sellwood, and J. S. Rowan (2003), Calcrete profile development in Quaternary alluvial sequences, southeast Spain: Implications for using calcretes as a basis for landform chronologies, *Earth Surf. Processes Landforms*, *28*, 169–185.

Cao, J., H. Yang, and Z. Kang (2011), Preliminary regional estimation of carbon sink flux by carbonate rock corrosion: A case study of the Pearl River Basin, *Chin. Sci. Bull.*, *56*, 3766–3773.

Cao, J., D. Yuan, C. Groves, F. Huang, H. Yang, and Q. Lu (2012), Carbon fluxes and sinks: The consumption of atmospheric and soil CO_2 by carbonate rock dissolution, *Acta Geologica Sinica*, *86*, 963–972.

Capo, R. C., and O. A. Chadwick (1999), Sources of strontium and calcium in desert soil and calcrete, *Earth Planet. Sci. Lett.*, *170*, 61–72.

Capo, R. C., C. E. Whipkey, J. R. Blachere, and O. A. Chadwick (2000), Pedogenic origin of dolomite in a basaltic weathering profile, Kohala peninsula, Hawaii, *Geology*, *28*(3), 271–274.

Carlos, B. A., S. J. Chipera, D. L. Bish, and S. J. Craven (1993), Fracture-lining manganese oxide minerals in silicic tuff, Yucca Mountain, Nevada, U.S.A, *Chem. Geol.*, *107*, 47–69.

Chiquet, A., A. Michard, D. Nahon, and B. Hamelin (1999), Atmospheric input vs in situ weathering in the genesis of calcretes: An Sr isotope study at Galvez (Central Spain), *Geochim. Cosmochim. Acta*, *63*, 311–323.

Chitale, J. D. (1986), Study of petrography and internal structures in calcretes of West Texas and New Mexico (Microtextures, Caliche), PhD dissertation thesis, 120 pp., Texas Tech University, Lubbock, Tex.

Curl, R. L. (2012), Carbon shifted but not sequestered, *Science*, *355*, 655.

Dart, R. C., K. M. Barovich, D. J. Chittleborough, and S. M. Hill (2007), Calcium in regolith carbonates of central and southern Australia: Its source and implications for the global carbon cycle, *Palaeogeogr. Palaeoclimatol. Palaeoecol.*, *249*, 322–334.

Decker, J. E., S. Niedermann, and M. J. De Wit (2011), Soil erosion rates in South Africa compared with cosmogenic 3HE-based rates of soil production, *S. Afr. J. Geol.*, *114*(3-4), 475–488.

Denniston, R. F., C. K. Shearer, G. D. Layne, and D. T. Vaniman (1997), SIMS analyses of minor and trace element distributions in fracture calcite form Yucca Mountain, Nevada, USA, *Geochim. Cosmochim. Acta*, *61*(9), 1803–1818.

Derry, L. A., and O. A. Chadwick (2007), Contributions from Earth's atmosphere to soil, *Elements*, *3*, 333–338.

Diaz-Hernandez, J. (2010), Is soil carbon storage underestimated?, *Chemosphere*, *80*, 346–349.

Dohrenwend, J. D., and A. J. Parsons (2009), Pediments in arid environments, in *Geomorphology of Desert Environments*, edited by A. J. Parsons and A. D. Abrahams, pp. 377–411, Springer, New York.

Dorn, R. I. (1995), Digital processing of back-scatter electron imagery: A microscopic approach to quantifying chemical weathering, *Geol. Soc. Am. Bull.*, *107*, 725–741.

Durand, N., Y. Gunnell, P. Curmi, and S. M. Ahmad (2006), Pathways of calcrete development on weathered silicate rocks in Tamil Nadu, India: Mineralogy, chemistry and paleoenvironmental implications, *Sediment. Geol.*, *192*, 1–18.

Durand, N., Y. Gunnell, P. Curmi, and S. M. Ahmad (2007), Pedogenic carbonates on Precambrian silicate rocks in South India: Origin and paleoclimatic significance, *Quat. Int.*, *162-163*, 35–49.

Eswaran, H., E. Van den Berg, and P. Reich (1993), Organic carbon in soils of the world, *Soil Sci. Soc. Am. J.*, *57*, 192–194.

Eswaran, H., P. F. Reich, J. M. Kimble, F. H. Beinroth, E. Padmanabhan, and P. Moncharoen (1999), Global carbon stocks, in *Global Climate Change and Pedogenic Carbonates*, edited by R. Lal et al., pp. 15–25, Lewis Publishers, Boca Raton, Fla.

Falkowski, P., et al. (2007), The global carbon cycle: A test of our knowledge of Earth as a system, *Science*, *290*, 291–296.

Fletcher, K. E. K., T. K. Rockwell, and W. D. Sharp (2011), Late Quaternary slip rate of the southern Elsinore Fault, Southern California: Dating offset alluvial fans via 230Th/U on pedogenic carbonate, *J. Geophys. Res.*, *116*, F02006, doi:10.1029/02010JF001701.

Goldstein, J., D. E. Newbury, D. C. Joy, C. E. Lyman, P. Echlin, E. Lifshin, T. L. Sawyer, and J. R. Michael (2003), *Scanning Electron Microscopy and X-ray Microanalysis*, pp. 586, Elsevier, Amsterdam.

Goudie, A. S. (2003), *Great Warm Deserts of the World: Landscapes and Evolution*, pp. 480, Oxford Univ. Press, New York.

Hamidi, E. M., Y. Geraud, F. Colin, and B. Boulange (1999), Analyse de la porosite dans un profil d'encroutment carbonate sur les basaltes du Trias du Moyen Atlas (Maroc), *C. R. Acad. Sci., Ser. IIa: Sci. Terre Planets*, *329*, 351–356.

Hamidi, E. M., F. Colin, A. Michard, B. Boulange, and D. Nahon (2001), Isotopic tracers of the origin of Ca in a carbonate crust from the Middle Atlas, Morocco, *Chem. Geol.*, *176*, 93–104.

Heaton, T. J., P. G. Blackwell, and C. E. Buck (2009), A Bayesian approach to the estimation of radiocarbon calibration curves: The INTCAL09 methodology, *Radiocarbon*, *51*, 1151–1164.

Heilweil, V. M., T. S. McKinney, M. S. Zhdanov, and D. E. Watt (2007), Controls on the variability of net infiltration to desert sandstone, *Water Resour. Res.*, *43*, W07431, doi:10.1029/02006WR005113.

Heimsath, A. M., J. Chappell, W. E. Dietrich, K. Nishiizumi, and R. C. Finkel (2001), Late Quaternary erosion in southeastern Australia: A field example using cosmogenic nuclides, *Quat. Int.*, *83-85*, 169–185.
Heimsath, A. M., J. Chappell, W. E. Dietrich, K. Nishiizumi, and R. C. Finkel (2006a), Soil production on a retreating escarpment in southeastern Australia, *Geology*, *28*, 787–790.
Heimsath, A. M., J. Chappell, R. Finkel, K. Fifield, and A. Alimanovic (2006b), Escarpment erosion and landscape evolution in southeastern Australia, *Geol. Soc. Am. Special Paper*, *398*, 173–190.
Hill, S. M., G. Taylor, and K. G. McQueen (1998), Genesis of some calcretes in the southern Yilgarn Craton, Western Australia: Implications for mineral exploration—Discussion, *Aust. J. Earth Sci.*, *45*, 177–178.
Hunt, A. G., and J. Q. Wu (2004), Climatic influences on Holocene variations in soil erosion rates on a small hill in the Mojave Desert, *Geomorphology*, *58*, 263–289.
Hurley, B., S. Welte, W. King, D. Gilewitch, and J. Brockhaus (2004), *Desert Analysis: The Quest for Training Areas*, pp. 37, Center for Environmental and Geographical Sciences, U.S. Military Academy, West Point, NY.
Jacobson, A. D., J. D. Blum, C. P. Chamberlain, M. A. Poage, and V. F. Sloan (2002a), Ca/Sr and Sr isotope systematics of a Himalayan glacial chronosequence: Carbonate versus silicate weathering rates as a function of land surface age, *Geochim. Cosmochim. Acta*, *66*, 13–27.
Jacobson, A. D., J. D. Blum, and L. M. Walter (2002b), Reconciling the elemental and Sr isotope composition of Himalayan weathering fluxes: Insights from the carbonate geochemistry of stream waters, *Geochim. Cosmochim. Acta*, *66*, 3417–3429.
Klappa, C. F. (1979), Lichen stromatolites: Criterion for subaerial exposure and a mechanism for the formation of laminar calcretes (caliche), *J. Sediment. Petrol.*, *49*, 387–400.
Knauth, L. P., M. Brilli, and S. Klonowski (2003), Isotope geochemistry of caliche developed on basalt, *Geochim. Cosmochim. Acta*, *67*, 185–195.
Kounov, A., S. Niedermann, M. J. De Wit, G. Viola, M. Andreoli, and J. Erzinger (2007), Present denundation rates at selected sections of the South African escarpment and the elevated continental interior based on cosmogenic 3He and 21Ne, *S. Afr. J. Geol.*, *110*, 235–248.
Krinsley, D. H., and C. R. Manley (1989), Backscattered electron microscopy as an advanced technique in petrography, *J. Geol. Educ.*, *37*, 202–209.
Kump, L. R., S. L. Brantley, and M. A. Arthur (2000), Chemical weathering, atmospheric CO_2, and climate, *Annu. Rev. Earth Planet. Sci.*, *28*, 611–667.
Lal, R. (2004), Soil carbon sequestration impacts on global climate change and food security, *Science*, *304*, 1623–1627.
Lal, R. (2008), Sequestration of atmospheric CO_2 in global carbon pools, *Energy Environ. Sci.*, *1*, 86–100.
Lerman, A., and F. T. MacKenzie (2005), CO_2 Air-Sea exchange due to calcium carbonate and organic matter storage, and its implications for the global carbon cycle, *Aquat. Geochem.*, *11*, 345–390.
Lian, B., D. X. Yuan, and Z. H. Liu (2011), Effect of microbes on karstification in karst ecosystems, *Chin. Sci. Bull.*, *56*, 3743–3747.
Liu, S., N. Bliss, E. T. Sundquist, and T. G. Huntington (2003), Modeling carbon dynamics in vegetation and soil under the impact of soil erosion and deposition, *Global Biogeochem. Cycles*, *17*(2), 1074, doi:10.1029/2002GB002010.
Liu, Z., W. Dreybrodt, and H. Wang (2010), A new direction in effective accounting for the atmospheric CO1 budget: Considering the combined action of carbonate dissolution, the global water cycle and photosynthetic uptake of DIC by aquatic organisms, *Earth Sci. Rev.*, *99*, 162–172.
Liu, Z., W. Dreybrodt, and H. Liu (2011), Atmospheric CO_2 sink: Silicate weathering or carbonate weathering?, *Appl. Geochem.*, *26*, S292–S294.
Machette, M. N. (1985), Calcic soils of the southwestern United States, *Geol. Soc. Am. Special Paper*, *203*, 1–21.
McAuliffe, J. R., and T. R. Van Devender (1998), A 22,000-year record of vegetation change in the north-central Sonoran Desert, *Palaeogeogr. Palaeoclimatol. Palaeoecol.*, *141*, 253–275.
McPherson, B. J., and E. T. Sundquist (Eds.) (2009), *Carbon Sequestration and Its Role in the Global Carbon Cycle*, pp. 358, AGU, Washington, D. C.
McQueen, K. G., S. M. Hill, and K. A. Foster (1999), The nature and distribution of regolith carbonate accumulations in southeastern Australia and their potential as a sampling medium in geochemical exploration, *J. Geochem. Explor.*, *67*, 67–82.
Meigs, P. (1953), World distribution of arid and semi-arid homoclimtes, in *Review of Research on Arid Zone Hydrology*, edited by A. Z. Programme, pp. 203–209, UNESCO, Paris.
Monger, H. C., and R. A. Gallegos (2000), *Biotic and Abiotic Processes and Rates of Pedogenic Carbonate Accumulation in the Southwestern United States—Relationship to Atmospheric CO2 Sequestration*, Global climate change and pedogenic carbonates, pp. 273–289, CRC, Boca Raton, Fla.
Moore, C. H. (1989), *Carbonate Diagenesis and Porosity*, pp. 338, Elsevier, Amsterdam.
Naiman, Z., J. Quade, and P. J. Patchett (2000), Isotopic evidence for eolian recycling of pedogenic carbonate and variations in carbonate dust sources throughout the Southwest United States, *Geochim. Cosmochim. Acta*, *64*, 3099–3109.
Nash, D. J., and S. J. McLaren (2003), Kalahari valley calcretes: Their nature, origin, and environmental significance, *Quat. Int.*, *111*, 3–22.
Neymark, L. A., Y. Amelin, J. B. Paces, and Z. E. Peterman (2002), U-Pb ages of secondary silica at Yucca Mountain, Nevada: Implications for the paleohydrology of the unsaturated zone, *Appl. Geochem.*, *17*, 709–734.
Neymark, L. A., J. B. Paces, B. D. Marshall, Z. E. Peterman, and J. F. Whelan (2005), Geochemical and C,O,Sr, and U-series isotopic evidence for the meteoric origin of calcrete at Solitario Wash, Crater Flat, Nevada, USA, *Environ. Geol.*, *48*(4-5), 450–465.
Nichols, K. K., P. R. Bierman, M. C. Eppes, M. Caffee, R. Finkel, and J. Larsen (2005), Late Quaternary history of the Chemehuevi Mountain Piedmont, Mojave Desert, deciphered using 10Be and 26Al, *Am. J. Sci.*, *305*, 345–368.
Peterman, Z. E., J. S. Stuckless, B. D. Marshall, S. A. Mahan, and K. Futa (1992), Strontium isotope geochemistry of calcite fracture fillings in deep core, Yucca Mountain, Nevada—A progress report, in *High Level Radioactive Waste Management*, pp. 1582–1586, American Society of Civil Engineers, New York.
Quade, J., A. R. Chivas, and M. T. MCCulloch (1995), Strontium and carbon isotope tracers and the origins of soil carbonate in South Australia and Victoria, *Palaeogeogr. Palaeoclimatol. Palaeoecol.*, *113*, 103–117.
Quade, J., N. Enligsh, and P. G. DeCelles (2003), Silicate versus carbonate weathering in the Himalaya: A comparison of the Arun and Seti River watersheds, *Chem. Geol.*, *202*, 275–296.
Rasmussen, C. (2006), Distribution of soil organic and inorganic carbon pools by biome and soil taxa in Arizona, *Soil Sci. Soc. Am. J.*, *70*, 256–265.
Schlesinger, W. H. (1982), Carbon storage in the caliche of arid soils: A case study from Arizona, *Soil Sci.*, *133*, 247–255.
Schlesinger, W. H. (1985), The formation of caliche in soils of the Mojave Desert, California, *Geochim. Cosmochim. Acta*, *49*, 57–66.
Sombroek, W. G., F. O. Nachtergaele, and A. Hebel (1993), Amounts, dynamics and sequestering of carbon in tropical and subtropical soils, *Ambio*, *22*, 417–426.
Schwartzman, D. W. (1999), *Life, Temperature and the Earth: The Self-Organizing Biosphere*, 241 pp., Columbia Univ. Press, New York.
Stadelman, S. (1994), Genesis and post-formational systematics of carbonate accumulations in Quaternary soils of the southwestern United States, PhD dissertation, 124 pp., Texas Tech University, Lubbock, Tex.

Stokes, M., D. J. Nash, and A. M. Harvey (2006), Calcrete "fossilisation" of alluvial fans in SE Spain: The roles of groundwater, pedogenic processes and fan dynamics in calcrete development, *Geomorphology*, *85*, 63–84.

Stuckless, J. S., Z. E. Peterman, and D. R. Muhs (1991), U and Sr isotopes in ground water and calcite, Yucca Mountain, Nevada: Evidence against upwelling water, *Science*, *254*, 551–554.

Suchet, P. A., J. Probst, and W. Ludwig (2003), Worldwide distribution of continental rock lithology: Implications for the atmospheric/soil CO_2 uptake by continental weathering and alkalinity river transport to the oceans, *Global Biogeochem. Cycles*, *17*(2), 1038, doi:10.1029/2002GB001891.

Sundquist, E. T. (1993), The global carbon dioxide budget, *Science*, *259*, 934–941.

Sundquist, E. T., R. C. Burruss, S. Faulkner, R. Gleason, J. Harden, Y. Kharaka, L. Tieszen, and M. Waldrop (2008), *Carbon Sequestration to Mitigate Climate Change*, 4 pp., U.S. Geological Survey, Washington, D. C.

Sundquist, E. T., K. V. Ackerman, L. Parker, and D. N. Huntzinger (2009), An introduction to global carbon cycle management, in *Carbon Sequestration and Its Role in the Global Carbon Cycle*, *Geophys. Monogr. Ser.*, edited by B. J. McPherson and E. T. Sundquist, pp. 1–23, AGU, Washington, D. C.

Szabo, B. J., and T. K. Kyser (1990), Ages and stable-isotope compositions of secondary calcite and opal in drill cores from Tertiary volcanic rocks of the Yucca Mountain area, Nevada, *Geol. Soc. Am. Bull.*, *102*, 1714–1719.

Tipper, E. T., M. J. Bickle, A. Galy, A. J. West, C. Pomiès, and H. J. Chapman (2006), The short term climatic sensitivity of carbonate and silicate weathering fluxes: Insight from seasonal variations in river chemistry, *Geochim. Cosmochim. Acta*, *70*, 2737–2754.

Urey, H. C. (1952), *The Planets, Their Origin and Development*, 245 pp., Yale Univ. Press, New Haven, Conn.

Van Devender, T. R., R. S. Thompson, and J. L. Betancourt (1987), *Vegetation History of the Deserts of Southwestern North America; The Nature and Timing of the Late Wisconsin-Holocene Transition*, pp. 323–352, Geological Society of America, Boulder, Colo.

Vaniman, D. T., and S. J. Chipera (1996), Paleotransport of lanthanides and strontium recorded in calcite compositions from tuffs at Yucca Mountain, Nevada, *Geochim. Cosmochim. Acta*, *60*, 4417–4433.

Verrecchia, E. P. (1990), Litho-diagenetic implications of the calcium oxalate-carbonate biogeochemical cycle in semiarid calcretes, Nazareth, Israel, *Geomicrobiol. J.*, *8*, 87–99.

Violette, A., et al. (2010), Formation and preservation of pedogenic carbonates in South India, links with paleo-monsoon and pedological conditions: Clues from Sr isotopes, U–Th series and REEs, *Geochim. Cosmochim. Acta*, *58*, 7059–5085.

Wang, Y., R. Amundson, and S. Trumbore (1994), A model for soil (CO_2) C-14 and its implications for using C-14 to date pedogenic carbonate, *Geochim. Cosmochim. Acta*, *58*, 393–399.

Watts, N. L. (1980), Quaternary pedogenic calcretes from the Kalahari (southern Africa): Mineralogy, genesis and diagenesis, *Sedimentology*, *27*, 661–686.

Whelan, J. F., and J. S. Stuckless (1992), Paleohydrologic implications of the stable isotope composition of secondary calcite within Yucca Mountain, Nevada, in *International High Level Radioactive Waste Management*, pp. 1572–1581, American Nuclear Society, La Grange Park, IL, Las Vegas, Nev.

Whelan, J. F., D. T. Vaniman, J. S. Stuckless, and R. J. Moscati (1994), Paleoclimatic and paleohydrological records from secondary calcite: Yucca Mountain, Nevada, in *High Level Radioactive Waste Management*, pp. 2738–2745, American Society of Civil Engineers, New York.

Whelan, J. F., J. B. Paces, and Z. E. Peterman (2002), Physical and stable-isotope evidence for formation of secondary calcite and silica in the unsaturated zone, Yucca Mountain, Nevada, *Appl. Geochem.*, *17*, 735–350.

Wilson, N. S. F., J. S. Cline, and Y. V. Amelin (2003), Origin, timing, and temperature of secondary calcite-silica mineral formation at Yucca Mountain, Nevada, *Geochim. Cosmochim. Acta*, *67*, 1145–1176.

Winter, B. L., and L. P. Knauth (1992), Stable isotope geochemistry of carbonate fracture fills in Montery Formation, California, *J. Sediment. Res.*, *62*, 208–219.

Yang, R., Z. H. Liu, C. Zeng, and M. Zhao (2012), Response of epikarst hydrochemical changes to soil CO_2 and weather conditions at Chenqi, Puding, SW China, *J. Hydrol.*, *468*, 151–158.

Zhang, C. (2011), Carbonate rock dissolution rates in different land uses and their carbon sink effect, *Chin. Sci. Bull.*, *56*, 3759–3765.